

# Preparation and detection of d-wave superfluidity in two-dimensional optical superlattices

A. M. Rey<sup>1</sup>, R. Sensarma<sup>2</sup>, S. Foelling<sup>2</sup>, M. Greiner<sup>2</sup>, E. Demler<sup>1,2</sup> and M.D. Lukin<sup>1,2</sup>

<sup>1</sup> *Institute for Theoretical Atomic, Molecular and Optical Physics,*

*Harvard-Smithsonian Center of Astrophysics, Cambridge, MA, 02138. and*

<sup>2</sup> *Physics Department, Harvard University, Cambridge, Massachusetts 02138, USA*

We propose a controlled method to create and detect d-wave superfluidity with ultracold fermionic atoms loaded in two-dimensional optical superlattices. Our scheme consists in preparing an array of nearest-neighbor coupled square plaquettes or “superplaquettes” and using them as building blocks to construct a d-wave superfluid state. We describe how to use the coherent dynamical evolution in such a system to experimentally probe the pairing mechanism. We also derive the zero temperature phase diagram of the fermions in a checkerboard lattice (many weakly coupled plaquettes) and show that by tuning the inter-plaquette tunneling spin-dependently or varying the filling factor one can drive the system into a d-wave superfluid phase or a Cooper pair density wave phase. We discuss the use of noise correlation measurements to experimentally probe these phases.

arXiv:0806.0166v1 [cond-mat.other] 2 Jun 2008

Ultracold atoms in optical lattices[1] are promising simulators of complex many-body problems and model Hamiltonians that arise in condensed matter physics. They provide a clean system with parameters which can be tuned in a controlled fashion from the weakly interacting to the strongly interacting limits. The observation of the superfluid to Mott insulator transition with bosons[2] and recent experimental realization of both repulsive and attractive Hubbard models[3, 4] with Fermions are important steps in that direction. Recently, the existence of superexchange antiferromagnetic correlations have been shown in an array of isolated double wells[5, 6]. Here we extend similar considerations for a d-wave superfluid state and propose an experimental scheme to realize and detect it.

The repulsive Hubbard model on a square lattice is one of the most important model Hamiltonians for strongly interacting fermions and is widely believed to contain the essential features of high temperature superconductors[7]. At half filling (one fermion per site), strong repulsion leads to localization of the fermions resulting in a Mott insulator. Superexchange interactions lead to an antiferromagnetic ground state. Away from half filling, antiferromagnetic correlations compete with the kinetic energy of the holes and the phase diagram remains unknown. Although there is no rigorous proof of existence of superfluidity in this model, approximate theoretical and Monte Carlo simulations at high temperatures [8] have conjectured the presence of d-wave superfluid ground states away from half-filling.

It has been known for some time[9] that the minimal 2D unit that can sustain d-wave pairing physics is a single square plaquette (see Fig.1). The single plaquette has been the starting point of various approaches[10, 11, 12, 13] to the Hubbard model on the square lattice. Even with purely repulsive interactions, there is a range of parameters where two holes tend to bind together on a single plaquette rather than to delocalize among different plaquettes. The hole pair that is created has a d-wave symmetry and can lead to d-wave superfluidity once the plaquettes are coupled.

We first propose an experimental scheme to verify these concepts by creating an array of isolated super-plaquettes (i.e.

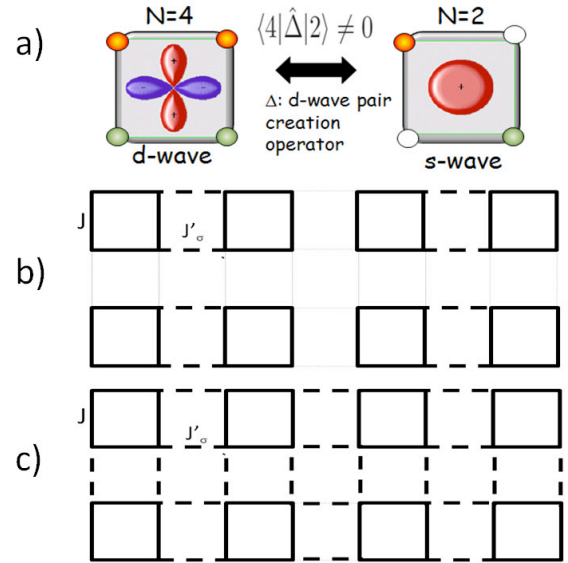


FIG. 1: A plaquette is the minimum system that exhibits d-wave symmetry. a) When loaded with four fermions the ground state is d wave symmetric while when loaded with 2 the ground state exhibits s wave symmetry. Consequently the two states have non zero matrix element with the d-wave pair creation operator. Here we consider the situations when plaquettes are coupled into a super-plaquette array and into a checkerboard array, which are schematically represented in b) and c) respectively. In the picture the spin independent intra-plaquette tunneling  $J$  is represented by a thick solid line and the inter-plaquette tunneling,  $J'_\sigma \ll J$  by a dashed line. The subscript  $\sigma$  in  $J'_\sigma$  emphasizes that it can depend on the spin of the atom.

two adjacent plaquettes coupled by a weak tunneling, see Fig. 1b) and loading them with six Fermions each. To measure the binding energy of the hole pair, we analyze the coherent dynamics of the super-plaquette. Finally we derive the phase diagram of the weakly coupled plaquettes with spin-dependent inter-plaquette tunneling. We show that the system can be driven to either a d-wave superfluid or a density wave state[13]. We propose an experimental scheme to realize this and discuss the detection of the two quantum phases via atomic noise correlations measurements[14, 15, 16, 17, 18].

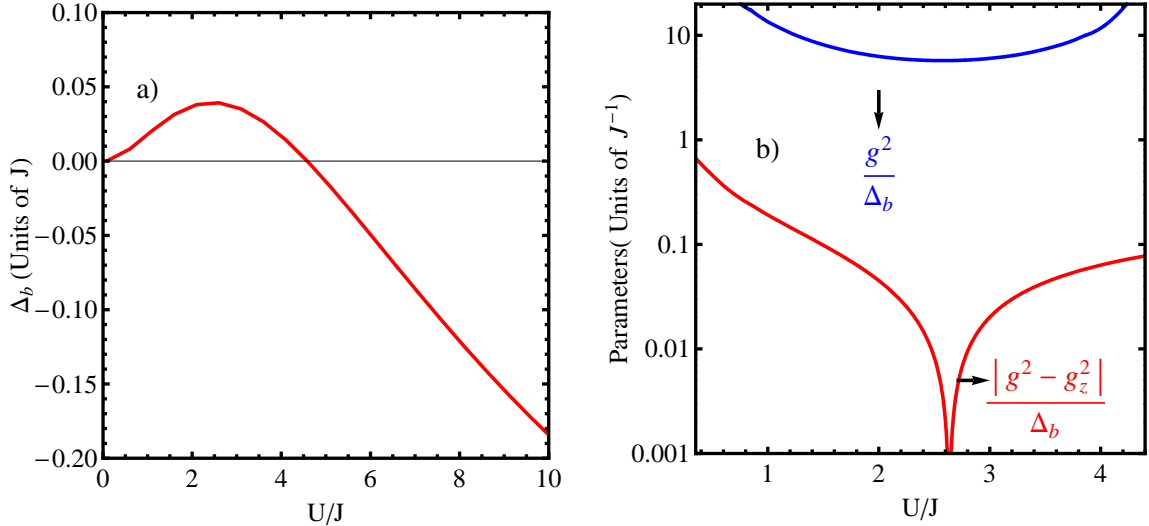


FIG. 2: a) The red solid line corresponds to the pair binding energy in a plaquette. For  $0 < U/J < 4.6$ ,  $\Delta_b > 0$  and consequently it is energetically favorable to have two holes in the same plaquette. b) Coupling parameters as function of  $U/J$  for the effective XXZ Hamiltonian, Eq. (5). The blue line corresponds to  $g^2/\Delta_b$  as a function of  $U/J$ . This is the only parameter that appears in the super-plaquette Hamiltonian. When more than two plaquettes are coupled, new virtual processes have to be accounted for which change the Ising term coupling constant. While the latter become proportional to  $g_z^2/\Delta_b$ , the transverse coupling constant remains the same, i.e. proportional to  $g^2/\Delta_b$ . The red line shows the absolute value of the difference between these two parameters.

## I. PLAQUETTE FERMION MODELS

Consider fermions in an isolated plaquette (shown in Fig.1a). Assuming one accessible single particle state in each well (i.e. level spacing much larger than other energy scales in the problem), the system is described by the Hubbard Hamiltonian

$$\hat{H} = -J \sum_{\langle r, r' \rangle, \sigma} \hat{c}_{r\sigma}^\dagger \hat{c}_{r'\sigma} + U \sum_r \hat{n}_{r\uparrow} \hat{n}_{r\downarrow}, \quad (1)$$

where  $J$  is the tunneling matrix element and  $U$  is the onsite Hubbard repulsion. Here  $\hat{c}_{r\sigma}$  are fermionic annihilation operators,  $\hat{n}_{r\sigma} = \hat{c}_{r\sigma}^\dagger \hat{c}_{r\sigma}$  are number operators,  $r = 1, \dots, 4$ , labels the four sites in a plaquette and the term  $\langle r, r' \rangle$  indicates that the sum is restricted to nearest neighbors.

The eigenstates in a single plaquette depend on the filling factor. When filled with  $N = 4$  or  $N = 2$  fermions, the ground state is a spin-singlet exhibiting  $d$  and  $s$  wave symmetry respectively. We denote the corresponding ground states as  $|4\rangle$  and  $|2\rangle$  (See Fig.1a). On the other hand, for  $N = 3$ , the ground state is degenerate with  $S = 1/2$  and  $p_x \pm ip_y$  symmetry in the regime  $U < U_t \sim 18.6J$ . We denote them as  $|3^{(\sigma, \tau)}\rangle$  with  $\sigma$  and  $\tau$  specifying the spin polarization and the orbital "chirality" ( $\tau = \pm$ ). The  $d$  vs  $s$  wave symmetry of the  $|4\rangle$  and  $|2\rangle$  states is the crucial element in obtaining the  $d$ -wave pairing mechanism, and the hole-pair creation operator that connects the two states must have a  $d$ -wave symmetry[9];

i.e.  $\langle 2 | \hat{\Delta}_d^\dagger | 4 \rangle \neq 0$ , where

$$\hat{\Delta}_d = (\hat{s}_{12} + \hat{s}_{34} - \hat{s}_{14} - \hat{s}_{23})/2, \quad (2)$$

and  $\hat{s}_{rr'} = (\hat{c}_{r\uparrow}^\dagger \hat{c}_{r'\downarrow}^\dagger - \hat{c}_{r\downarrow}^\dagger \hat{c}_{r'\uparrow}^\dagger)/\sqrt{2}$  creates a singlet on the  $rr'$  bond.

We next look at the case of 2 holes in two isolated plaquettes. The holes can bind together within the same plaquette or separate as single holes in each plaquette depending on the binding energy defined as

$$\Delta_b = 2E_g(N=3) - E_g(N=4) - E_g(N=2) \quad (3)$$

being positive or negative respectively. Here  $E_g(N=n)$  is the single plaquette ground state energy when loaded with  $n$  atoms. As shown in Fig. 2,  $\Delta_b$  is a non-monotonic function of  $U/J$  [11, 12, 13, 19], which reaches a maximum value of  $\Delta_b \approx 0.04J$  at  $U \approx 2.45J$  and becomes negative for  $U = U_c > 4.58J$ . Consequently only when  $U < U_c$  hole pairs on a single plaquette are energetically stable.

Two adjacent plaquettes can be coupled through a weak (possibly spin dependent) tunneling  $J'_\sigma$  to form a super-plaquette (see Fig.1). As long as  $0 < J'_\sigma \ll \Delta_b$ , the states  $|4, 2\rangle$  and  $|2, 4\rangle$  are lower in energy and occupation of the states  $|3^{(\sigma, \tau)}\rangle, 3^{(\bar{\sigma}, \bar{\tau})}\rangle$  are energetically suppressed. They can only be populated as "virtual" intermediate states leading to an effective super-exchange interaction between  $|4, 2\rangle$  and  $|2, 4\rangle$ . Specifically, by treating the  $|4\rangle$  and  $|2\rangle$  states as the pseudo-spin components  $|\uparrow\rangle$  and  $|\downarrow\rangle$  of an effective spin  $1/2$  system, the interaction between the effective spins can be described by

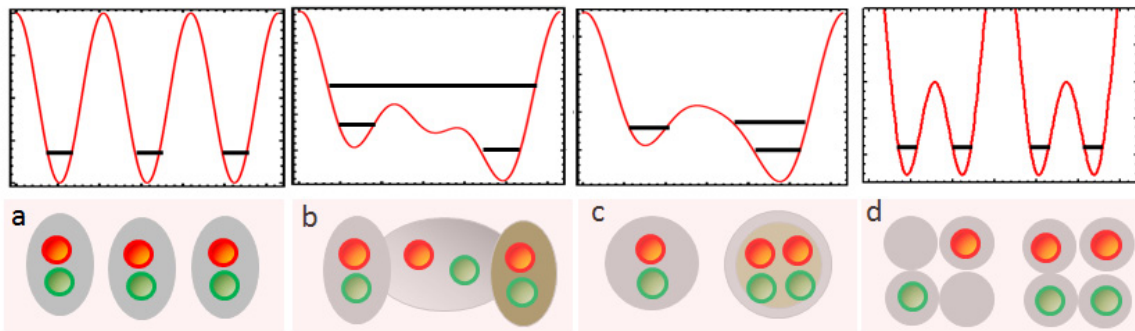


FIG. 3: Loading of fermions in a patterned loading array of plaquettes: a) First a unit filled band insulator of fermionic atoms is prepared in a rectangular lattice with lattice period  $4/3\lambda$  and  $2\lambda$  along the  $x$  and  $y$  direction respectively. b) A phase shifted  $4\lambda$  lattice along the  $x$  axis is slowly ramped up. c) As the period  $4/3\lambda$  lattice is ramped down, the period  $2\lambda$  lattice is ramped down generating a double well lattice. The bias is chosen such that the ground state has four fermions in the right and two fermions in the left sites of each double well. d) The lattice depth of the  $2\lambda$  lattice is increased to make all wells independent. Subsequently the bias is turned off and the isolated wells split into two. The overall scheme creates an array of independent plaquettes loaded in the ground state with alternating filling factors of 2 and 4 along the  $x$  direction.

an XXZ-type Hamiltonian

$$H_{eff} = -\frac{J'_\uparrow J'_\downarrow g^2}{\Delta_b} (\sigma_R^x \sigma_L^x + \sigma_R^y \sigma_L^y) + \frac{g^2 (J'^2_\uparrow + J'^2_\downarrow)}{2\Delta_b} \sigma_R^z \sigma_L^z \quad (4)$$

with  $\sigma_{i=R,L}^{\alpha=x,y,z}$  standard Pauli matrices acting on the right (R) or left (L) effective pseudo-spins and  $g$  the coupling matrix element between the right and left plaquettes which is of order one (see Fig.2).

Eq.(4) contains the essential physics we are interested in this work. If  $J'_\uparrow = J'_\downarrow$  the energy eigenstates are effective triplet and singlet states  $|t, s\rangle = \frac{1}{\sqrt{2}}(|4, 2\rangle \pm |2, 4\rangle)$  with the triplet being the ground state. These are separated by an energy gap  $\sim \Delta_b$  from the rest of the Hilbert space. The ground state has a non zero expectation value of the  $d$ -wave pair correlation operator  $\langle t | \hat{\Delta}_R^\dagger \hat{\Delta}_L | t \rangle \neq 0$  which leads to a  $d$ -wave superfluid when coupling all the plaquettes. On the contrary if  $J'_\uparrow \ll J'_\downarrow$ , the Ising term dominates and any infinitesimal symmetry-breaking perturbation will collapse the state into  $|4, 2\rangle$  or  $|2, 4\rangle$  which are inherently density-ordered states. These considerations indicate that the many body phase diagram of this model would depend on the spin-dependent couplings in a non-trivial way.

## II. PREPARATION AND DETECTION

To verify the energy structure of the hole-pair states we want to create an array of isolated super-plaquettes loaded with 2 and 4 fermions in the left and the right plaquettes respectively.

An array of plaquettes can be created by superimposing two orthogonal optical super-lattices formed by the superposition of two independent sinusoidal potentials which differ in periodicity by a factor of two [6, 20, 21]. The aim here is first to load the fermions in a 2D array of independent plaquettes with alternating filling factors of 4 and 2 along one direction.

The preparation procedure we propose is based on a unity-filled band insulator [22], and uses adiabatic manipulations of a super-lattice potential created by standing waves with four different periodicities  $\lambda$ ,  $2\lambda$ ,  $4\lambda$  and  $4\lambda/3$  (For other strategies see [12]). Such wavelength combinations are available for typical Fermionic atoms such as  $^{40}\text{K}$  and  $^6\text{Li}$  or can be engineered by intersecting four pairs of laser beams with appropriate angles [23], resulting in a set of four equidistant  $k$ -vectors. For the discussion we will also assume that there is a deep axial lattice that freezes the atom motion along the  $z$  direction.

The process of patterned loading an array of plaquettes is depicted in Fig.3. The initial band insulator is formed in a rectangular lattice with period  $4/3\lambda$  and  $2\lambda$  along the  $x$  and  $y$  directions, respectively. Adiabatically introducing a phase shifted  $4\lambda$  lattice along the  $x$  axis creates an effective  $4\lambda$ -lattice with three sites per cell with different energy offsets (See Fig.3). By ramping down the period  $4/3\lambda$  lattice while ramping up the period  $2\lambda$  one can convert the potential into a double well lattice with an asymmetric energy offset. This offset has to be large compared to the on-site repulsion to guarantee that the final ground state corresponds to a system with four fermions in the lower and two fermions in the higher sites of each double well. After increasing the lattice depth of the  $2\lambda$  lattice to suppress tunneling between the wells the bias can be removed and the isolated wells can be split into four sites by slowly turning on the  $\lambda$  lattice along both  $x$  and  $y$  directions. As a result, an array of independent plaquettes in the ground state with alternating filling factors of 4 and 2 along the  $x$  direction is created. To obtain an array of super-plaquettes, the tunneling between adjacent plaquettes can be controlled by the depth of the  $2\lambda$  potential, while the  $4\lambda$  lattice isolates super-plaquettes. The extra  $4\lambda/3$  lattice is needed to balance the offset created when the long lattice is added. Spin dependent control of the inter-plaquette tunneling can be achieved by additional control over the laser polarizations [21].

Under coherent quantum evolution, this system will exhibit

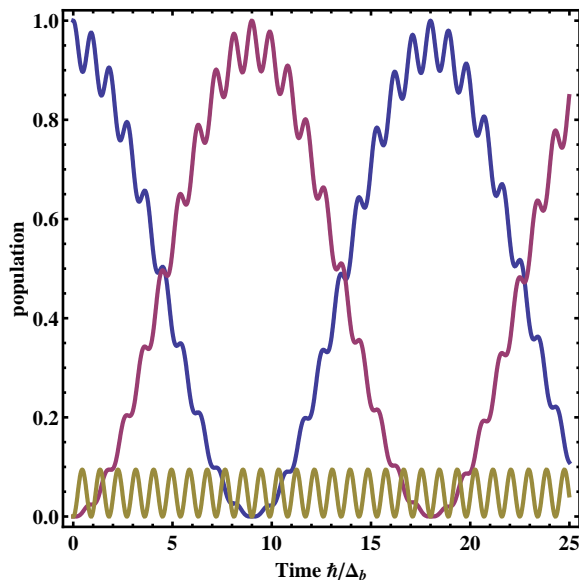


FIG. 4: Time evolution of the population of super-plaquettes in  $N_{42}(t)$  (blue),  $N_{24}(t)$  (purple) and  $N_{33}(t)$  (yellow) configurations respectively. The fast frequency component is determined by  $\Delta_b$  and the slow envelope by  $J'^2 g^2 / \Delta_b$ . Here  $U/J = 2.6$  and  $J'/J = 0.01$ .

Rabi oscillations between  $|4, 2\rangle$  and  $|2, 4\rangle$  states with the  $|3, 3\rangle$  populated virtually (as seen in Fig. 4). The frequency of oscillation of the envelope is given by  $4g^2 J'^2 / \Delta_b$  and can be used to measure the binding energy of the hole pairs. These ideas are similar to the ones used to measure the super-exchange energy in an array of double wells[5]. We next describe a method to measure the number of super-plaquettes in  $|4, 2\rangle$ ,  $|2, 4\rangle$  and  $|3, 3\rangle$  states using band-mapping techniques.

The distribution of super-plaquettes in different states can be obtained from the number distribution of fermions on the left and right plaquettes separately. To obtain the number distribution, after quenching  $J'$ , each plaquette is first converted to a single site by removing the short lattice potential. By counting the number of the atoms in each Brillouin zone after a band-mapping sequence on release from the lattice, the average occupation of all bands is determined. In a second step, the sequence is repeated, but the vibrational level of each atom on the right plaquette is increased by one after the conversion to a single well. This can be achieved in analogy to the scheme demonstrated in [24], by splitting the combined well and recombining in the presence of an energy bias. The bias is created using a phase shift on the 4-lambda lattice in such a way that only one of the plaquettes is affected. By comparing the resulting band occupations with those of step 1, the average filling of each band on each side is reconstructed. Both of these steps can be repeated with an additional Feshbach resonance sweep which converts all atom pairs to molecules. The remaining single atoms allow the separation of the fractions of even and the odd number states in each band of each side, which completes the determination of the plaquette atom number statistics.

From the obtained histogram of atom number distributions for the left and right plaquette at time  $t$ ,  $N_{42}(t)$ ,  $N_{24}(t)$  and

$N_{33}(t)$  can be determined[25] to measure the hole-pair binding energy.

### III. PHASE DIAGRAM ON CHECKERBOARD LATTICE

Now we study the more general case of a checkerboard array of plaquettes such as the one shown in Fig.1c. We will restrict our analysis to the regime  $|\Delta_b| \gg gJ_\sigma$  and  $\Delta_b > 0$  where we can treat the states  $|2\rangle$  and  $|4\rangle$  as the low energy modes and adiabatically eliminate high energy states via second order perturbation theory. This procedure yields a more general effective XXZ Hamiltonian given by

$$H_{eff} = \sum_{\langle \mathbf{R}, \mathbf{R}' \rangle} [-J^\perp (\sigma_{\mathbf{R}}^x \sigma_{\mathbf{R}'}^x + \sigma_{\mathbf{R}}^y \sigma_{\mathbf{R}'}^y) + J^z \sigma_{\mathbf{R}}^z \sigma_{\mathbf{R}'}^z] \quad (5)$$

where  $J^\perp = \frac{g^2 J'_\uparrow J'_\downarrow}{\Delta_b}$ ,  $J^z = (J_\uparrow'^2 + J_\downarrow'^2) \frac{g_z^2}{2\Delta_b}$ . Here we have neglected terms proportional to  $\sum_{\mathbf{R}} \sigma_{\mathbf{R}}^z$  since it is a conserved quantity in these systems. The coupling matrix element  $g_z$  has a complicated dependence on  $U/J$  as shown in Fig.2. For details about its derivation see methods.

The zero temperature phase diagram of the XXZ Hamiltonian is known and consequently can be used to infer the phase diagram of the corresponding fermionic system [13, 26, 27]. At 3/8 fermionic filling, i.e.  $N_4 = N_2$ , there is a second order phase transition as the  $J^z/J^\perp$  ratio is varied: While for  $J^z/J^\perp < 1$  the ground state corresponds to a gapless d-wave superfluid ( a magnetically ordered phase in the XY-plane for the effective spins), for  $J^z/J^\perp > 1$  it becomes a gapped Cooper pair density wave state, d-pdw (an antiferromagnetic order phase for the effective spins). The pdw state is not the usual particle-hole charge density wave state, but can be viewed as a crystal of d-wave Cooper pairs [28]. The point  $J^z = J^\perp$  is the critical point. In Fig. 5a, we show the phase diagram as a function of  $J'_\uparrow/J'_\downarrow$  where the tendency of anisotropic tunneling to stabilize the d-pdw phase can be observed. For the spin independent case  $J'_\uparrow = J'_\downarrow$ , our phase diagram is in agreement with the one obtained in Ref.[13], exhibiting a critical point at  $U_{cr} \sim 2.7J$ . Notice that since our analysis is based on the assumption that  $gJ' \ll \Delta_b$ , the parameter regime where it is applicable considerably reduces as one approaches the points  $U = 0$  and  $U/J \sim 4.6$  where  $\Delta_b$  vanishes.

Away from 3/8 fermionic filling, the phase diagram is almost insensitive to the  $J'_\uparrow/J'_\downarrow$  ratio. There is a first order phase transition from the d-pdw phase to the d-wave superfluid as the chemical potential is varied away from 3/8 filling. Due to the first order character of the transition, the d-pdw phase is surrounded by a small region where one observes phase coexistence [13, 27]. Except this region and the state at special filling factors: 1/4, 3/4, 1/2 and 1 when the system turns into an insulator, the low energy phase is always a gapless d-wave superfluid as shown in Fig. 5b.

To explore the different quantum phases, we propose to first prepare an initial array of isolated plaquettes, with the desired filling factor (see methods), and then slowly increase the inter-

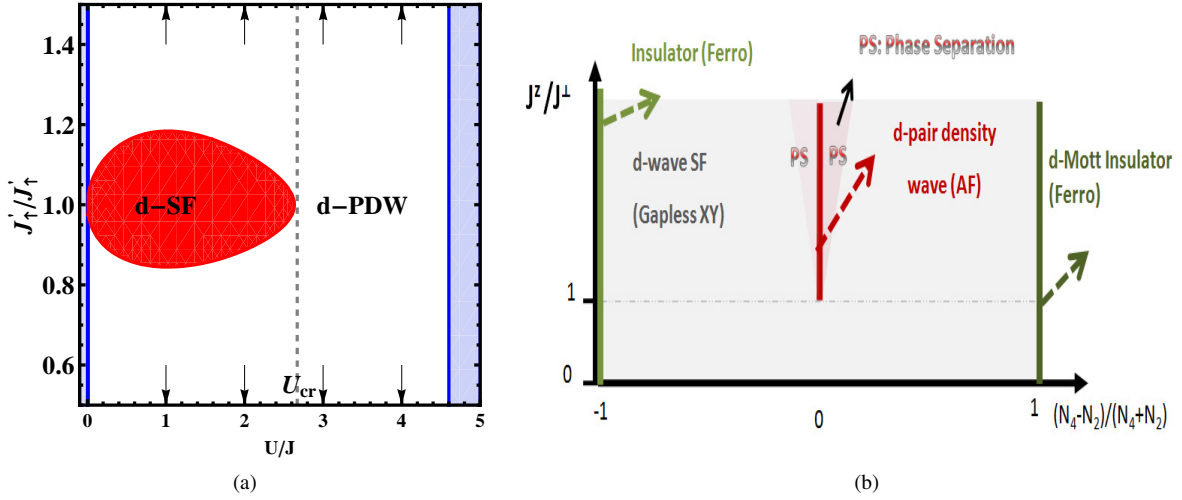


FIG. 5: a) Zero temperature phase diagram at  $3/8$  fermionic filling ( $N_4 = N_2 = N_{total}/2$ ). At this filling the system exhibits a second order phase transition from a d-wave Superfluid, d-SF, (magnetic ordered state in the XY plane for the effective spins) to a d-pair density wave state, d-pdw, (antiferromagnetic ordered phase for the effective spins) when the axial,  $J^z$ , and the transverse  $J^\perp$ , coupling constants that appear in the XXZ Hamiltonian become equal. As both  $J^\perp$  and  $J^z$  depend on the inter-plaquette tunnelings  $J'_{\uparrow,\downarrow}$  and the ratio  $U/J$ , the critical point can be controlled by tuning these microscopic parameters. b) Zero temperature phase diagram of the effective XXZ Hamiltonian as a function of the filling factor: Away from  $3/8$  fermionic filling ( $N_4 = N_2$ ), the d-wave superfluid phase is energetically favorable except at the fermionic filling factors  $1/4$  (or  $N_2 = N_{total}$ ) and  $1/2$  or ( $N_4 = N_{total}$ ) where the system becomes an insulator. There is an additional first order phase transition from a d-pdw to a d-Sf as the filling factor is varied away  $N_4 = N_2$  and this induces phase separation in a small range of filling factors around  $N_4 = N_2$ .

plaquette coupling taking advantage of the experimental ability to tune the lattice geometry and the ratio  $J^z/J^\perp$  by using spin dependent control. The effective XXZ Hamiltonian allows us to estimate the entropy of the ordered state (near  $T_c$ ) and hence the  $T/T_F$  of the initial trapped Fermi gas without the optical lattice required for observing these phases (assuming all later modifications are adiabatic). This gives an estimate of  $T/T_f \sim 0.01$  to observe the d-wave superfluid and  $T/T_f \sim 0.03$  to observe the charge ordered state. These values should be achievable with current technology.

#### IV. DETECTION OF THE QUANTUM PHASES VIA NOISE CORRELATIONS

Noise correlations [14] can be used to detect the different quantum phases. The atomic noise in an expanding cloud is related to the following four point functions at the time of the release:

$$G_{\mathbf{Q},\mathbf{Q}'}^{\sigma\sigma'} \propto \langle \hat{n}_{\mathbf{Q}\sigma} \hat{n}_{\mathbf{Q}'\sigma'} \rangle - \langle \hat{n}_{\mathbf{Q}\sigma} \rangle \langle \hat{n}_{\mathbf{Q}'\sigma'} \rangle \quad (6)$$

with  $\hat{n}_{\mathbf{Q}\sigma} \propto \sum_{l,s} e^{i\mathbf{Q}\cdot\mathbf{L}_{ls}} \langle c_{l\sigma}^\dagger c_{s\sigma} \rangle$ , being the quasi-momentum distribution and  $\mathbf{L}_{ls}$  a vector connecting the lattice sites  $s$  and  $l$ .  $G^{\sigma\sigma'}(\mathbf{Q}', \mathbf{Q})$  has the required ingredients to distinguish the two phases. On one hand,  $G^{\uparrow\downarrow}(\mathbf{Q}, \mathbf{Q}')$  contains terms proportional to  $|\langle \hat{\Delta} \rangle|^2$  (see Eq.2), and consequently a d-wave superfluid with  $\langle \hat{\Delta} \rangle \neq 0$  must exhibit interference fringes at  $\mathbf{Q} + \mathbf{Q}' = \mathbf{K}n$ ,  $\mathbf{K}$  being the reciprocal lattice vector of the plaquette array, which is half of the reciprocal lattice

vector of the underlying lattice. The  $d$  wave nature of the state will be signaled by a modulation of the peaks with an overall envelope with the characteristic d-wave nodal planes along  $Q_x = \pm Q_y$  and  $Q'_x = \pm Q'_y$  as shown in Fig.6. Information about the density order is given by  $G^{\uparrow\uparrow}$  which will show sharp dips at  $\mathbf{Q} - \mathbf{Q}' = (2n+1)\mathbf{K}/2$  in the presence of a d-pdw phase and a flat profile in the superfluid phase. In contrast to the unequal spin correlations,  $G^{\uparrow\uparrow}$  will not have the inherent  $d$ -wave symmetry. Equal spin correlations will also always exhibit dips at  $\delta(\mathbf{Q} - \mathbf{Q}' - n\mathbf{K})$  which reflect the characteristic anti-bunching of fermions [17]. Unfortunately, the amplitude of these dips can be about 30 times stronger than the dips at  $(2n+1)\mathbf{K}/2$  inherent from the charge density order (see Fig. 6b). This caveat can be avoided by quenching the kinetic energy of the atoms in the plaquettes before the release by slowly merging each plaquette into a single well. For details about the noise interference pattern we refer the reader to the method section.

#### V. CONCLUSIONS

In summary we have described a technique to prepare and detect d-wave superfluidity in ultra-cold fermionic systems loaded in optical super-lattices. Even though our theoretical predictions are restricted to a regime where perturbative expansions are valid, the ideas presented in this letter might open a window to explore in the laboratory more complex regimes which do not allow for a clear theoretical description. We point out that so far we have ignored the presence of any any

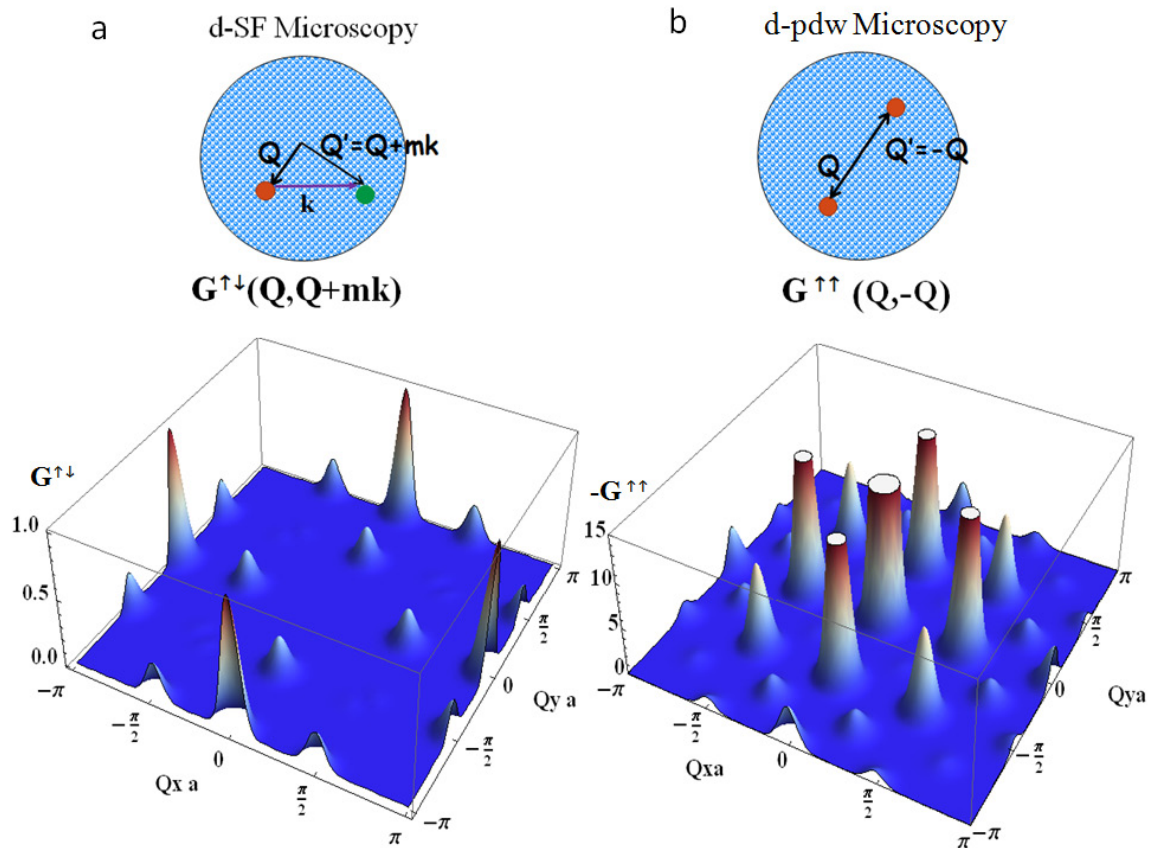


FIG. 6: The left panels display the unequal spin noise correlations,  $G^{\uparrow\downarrow}(\mathbf{Q}, \mathbf{Q}' = \mathbf{Q} + m\mathbf{k})$ , where  $\mathbf{k} = 2\pi/a\hat{x}$  is the reciprocal lattice vector of the underlying lattice with spacing  $a$ , assuming a  $d$ - wave superfluid. The right panel shows equal spin noise correlations (with opposite sign)  $-G^{\uparrow\uparrow}(\mathbf{Q}, \mathbf{Q}' = -\mathbf{Q})$  for a  $d$ -pdw state. Here we have subtracted the local density-density correlations within a plaquette (see methods).  $G^{\uparrow\downarrow}(\mathbf{Q}, \mathbf{Q}')$  exhibits interference peaks at  $\mathbf{Q} + \mathbf{Q}' = \mathbf{K}m$  in the  $d$ -wave superfluid regime with  $\mathbf{K} = \mathbf{k}/2$  is the reciprocal lattice vector of the plaquette array. The peaks are modulated by an overall envelope which probes the  $d$  wave symmetry. This modulation causes the disappearance of the peaks along the nodal lines  $Q_x = \pm Q_y$ . On the contrary  $-G^{\uparrow\uparrow}(\mathbf{Q}, -\mathbf{Q})$  exhibits interference peaks at  $\mathbf{Q} - \mathbf{Q}' = \mathbf{K}(2m + 1)/2$  in the  $d$ -pdw state. Due to the large kinetic energy of the fermions within a plaquette these peaks however are much weaker than the anti-bunching peaks, which always appear at  $\mathbf{Q} + \mathbf{Q}' = n\mathbf{K}$ .

inhomogeneous confining potential in the checkerboard lattice case. As the binding energy is a very sensitive quantity to any bias within a plaquette, its presence can certainly prevent the observation of the predicted phases. Consequently in this type of experiments it would be ideal to use a "box" type trapping

potential such as the one proposed in Ref.[31]

This work was supported by ITAMP, NSF (Career Program), Harvard-MIT CUA, AFOSR, Swiss NF, the Sloan Foundation, and the David and Lucille Packard Foundation.

- 
- [1] Bloch I., Dalibard J. and Zwerger W. Many-Body Physics with Ultracold Gases. Pre-print: arXiv:0704.3011.  
[2] Greiner, M. Mandel, O., Esslinger, T. Hänsch T. W. and Bloch, I. Quantum phase transition from a superfluid to a Mott insulator in a gas of ultracold atoms. Nature **415**, 39 (2002)  
[3] Strohmaier, N. *et al* Interaction-controlled transport of an ultracold Fermi gas. cond-mat:0707.3140  
[4] Jördens, R. Strohmaier, N. Günter, K. Moritz, H. and Esslinger, T. A Mott insulator of fermionic atoms in an optical lattice. cond-mat:0804.4009  
[5] Rey, A. M. Gritsev, V. Bloch, I. Demler, E. Lukin, M.D., Prepa-

- ration and detection of magnetic quantum phases in optical superlattices. Phys. Rev. Lett **99**, 140601 (2007).  
[6] Trotzky, S. *et al* Time-resolved Observation and Control of Superexchange Interactions with Ultracold Atoms in Optical Lattices. Science **319**, 295 (2008).  
[7] Anderson, P. W. The Resonating Valence Bond State in La<sub>2</sub>CuO<sub>4</sub> and Superconductivity. Science **235**, 1196 (1987)  
[8] Bickers, N.E. Scalapino, D.J. and White, S.R. Conserving Approximations for Strongly Correlated Electron Systems: Bethe-Salpeter Equation and Dynamics for the Two-Dimensional Hubbard Phys. Rev. Lett. **62**, 961(1989).

- [9] Scalapino, D.J. and Trugman, S. A. Local antiferromagnetic correlations and dx<sup>2</sup>-y<sup>2</sup> pairing Philos. Mag. B **74**, 607 (1996).
- [10] Morningstar, C.J. and Weinstein, M. Contractor renormalization group technology and exact Hamiltonian real-space renormalization group transformations. Phys. Rev. D. **54**, 4131(1996).
- [11] Altman, E. and Auerbach, A. Plaquette boson-fermion model of cuprates Phys. Rev. B **65**, 104508 (2002).
- [12] Trebst, S. Schollwöck, U. Troyer, M. and Zoller, P. d-Wave Resonating Valence Bond States of Fermionic Atoms in Optical Lattices Phys. Rev. Lett. **96**, 250402 (2006).
- [13] Yao, H. Tsai, W.F. and Kivelson, S. A. Myriad phases of the checkerboard Hubbard model Phys. Rev. B **76**, 161104(R) (2007).
- [14] Altman, E. Demler, E., and Lukin, M. D. Probing many-body states of ultracold atoms via noise correlations. Phys. Rev. A **70**, 013603 (2004).
- [15] Fölling S. *et al* Spatial quantum noise interferometry in expanding ultracold atom clouds. Nature **434**, 481 (2005).
- [16] Greiner, M. Regal, C. A. Ticknor, C. Bohn, J. L., and Jin, D. S. Detection of Spatial Correlations in an Ultracold Gas of Fermions Phys. Rev. Lett. **92**, 150405 (2004)
- [17] Rom T. *et al* Free fermion antibunching in a degenerate atomic Fermi gas released from an optical lattice. Nature **444**, 73 (2006)
- [18] Spielman, I. Phillips, W. D. and Porto, J. V. Mott-Insulator Transition in a Two-Dimensional Atomic Bose Gas. Phys. Rev. Lett. **98**, 080404 (2007)
- [19] Schumann, R. Thermodynamics of a 4-site Hubbard model by analytical diagonalization. Ann. Phys. **11**, 49 (2002).
- [20] Paredes, B. and Bloch, I. Minimum instances of topological matter in an optical plaquette. Phys. Rev. A **77**, 023603 (2008).
- [21] Sebby-Strabley, J. Anderlini, M. Jessen, P. S. and Porto, J. V. Lattice of double wells for manipulating pairs of cold atoms. Phys Rev A, **73**, 033605 (2006).
- [22] Köhl, M. Moritz, H. Stöferle, T. Gnter, K. and Esslinger, T. Fermionic Atoms in a Three Dimensional Optical Lattice: Observing Fermi Surfaces, Dynamics, and Interactions. Phys. Rev. Lett. **94**, 080403 (2005).
- [23] Peil, S. *et al* Patterned loading of a Bose-Einstein condensate into an optical lattice. Phys. Rev. A **67**, 051603(R) (2003).
- [24] Anderlini, M. Sebby-Strabley, J. Krus, J. Porto J.V. and Phillips, W.D. Controlled atom dynamics in a double-well optical lattice., J. Phys. B **39** S199S210(2006).
- [25] This assumes a good initial preparation, i.e. only the  $|4, 2\rangle$ ,  $|2, 4\rangle$  and  $|3, 3\rangle$  configurations are populated. In realistic situation defects might be present and additional measurements will be needed for a full reconstruction of left/right histograms.
- [26] Batrouni, G. and Scalettar, R. R. Phase Separation in Super-solids. Phys. Rev. Lett. **84**, 1599 (2000).
- [27] Hebert, F. *et al* Quantum phase transitions in the two-dimensional hardcore boson model Phys. Rev. B **65**, 014513 (2001).
- [28] Chen, H. D. Vafek, O. Yazdani A. and Zhang, S. C. Pair Density Wave in the Pseudogap State of High Temperature Superconductors Phys. Rev. Lett. **93**, 187002 (2004); Tesanovic, Z. Charge Modulation, Spin Response, and Dual Hofstadter Butterfly in High-Tc Cuprates. Phys. Rev. Lett. **93**, 217004 (2004); Pereg-Barnea, T. and Franz, M. Duality and the vibrational modes of a Cooper-pair Wigner crystal. Phys. Rev. B **74**, 014518 (2006).
- [29] K. Winkler *et al* Repulsively bound atom pairs in an optical lattice Nature **441**, 853 (2006).
- [30] S. Fölling *et al* Direct Observation of Second Order Atom Tun-

nelling. Nature, **448**, 1029 (2007).

- [31] T.P. Meyrath Schreck, F. Hanssen, J. L. Chuu, C.-S. and Raizen, M. G. Bose-Einstein condensate in a box. Phys. Rev. A, **71**, 041604(R)(2005).

## Methods

### Beyond the Effective Hamiltonian in a plaquette

The validity of the effective Hamiltonian, Eq.( 4) can be checked in the super-plaquette system by going one step beyond and deriving a more general effective Hamiltonian within the Hilbert subspace spanned by all the direct products of the low energy eigenstates of the isolated plaquette i.e  $|4, 2\rangle$ ,  $|2, 4\rangle$  and eight possible  $|3^{(\sigma, \tau)}, 3^{(\bar{\sigma}, \bar{\tau})}\rangle$  configurations. Even though in total there are 10 states only 4 of them are coupled by  $J'_\sigma$ . These are  $|t\rangle$ ,  $|+\rangle = \sum_{\sigma\tau} (-1)^{\sigma_z-1} |3^{(\sigma, \tau)}, 3^{(\bar{\sigma}, \bar{\tau})}\rangle/2$ ,  $|s\rangle$  and  $|-\rangle = \sum_{\sigma\tau} |3^{(\sigma, \tau)}, 3^{(\bar{\sigma}, \bar{\tau})}\rangle/2$ . In this basis the generalized effective Hamiltonian reduces to

$$H = \begin{pmatrix} 0 & -g\bar{J}' & 0 & 0 \\ -g\bar{J}' & \Delta_b & 0 & 0 \\ 0 & 0 & 0 & -g\delta J' \\ 0 & 0 & -g\delta J' & \Delta_b \end{pmatrix} \quad (7)$$

Here  $\delta J' = J'^\uparrow - J'^\downarrow$  and  $\bar{J}' = J'^\uparrow + J'^\downarrow$ . The Hamiltonian is block diagonal so the eigenstates are independent linear combinations of  $\{|t\rangle, |+\rangle\}$  and  $\{|s\rangle, |-\rangle\}$  respectively and have energies:

$$\begin{aligned} \hbar\omega_{1,3} &= \frac{\Delta_b \mp \sqrt{\Delta_b^2 + 4g^2\bar{J}'^2}}{2} \\ \hbar\omega_{2,4} &= \frac{\Delta_b \mp \sqrt{\Delta_b^2 + 4g^2\delta J'^2}}{2}. \end{aligned} \quad (8)$$

For  $gJ'_\sigma \ll |\Delta_b|$  the eigenstates are grouped in two doublets with common intra-doublet splitting  $4g^2J'^\uparrow J'^\downarrow/\Delta_b$  and doublet splitting  $\sim \Delta_b$ . The sign of  $\Delta_b$  determines which one of the two doublets is higher in energy. Since first order tunneling transfers amplitudes across the two doublets, if  $gJ'_\sigma \ll |\Delta_b|$ , these processes are energetically costly and only second order processes within the doublets are relevant. This assumption yields the effective spin Hamiltonian, Eq.(4). On the contrary for  $gJ'_\sigma \sim |\Delta_b|$  there is no clear energy separation between the doublets and the ground state is a mixture of the various independent plaquette states.

The corrections from the effective Hamiltonian can be measured by probing the coherent dynamical evolution proposed in the main text. In the weak coupling regime  $N_{24}(t)$  and  $N_{42}(t)$  will exhibit nice sinusoidal oscillations with a frequency proportional to  $g^2J'^2/\Delta_b$ . However for  $\Delta_b \sim J'$  a more complex dynamics will occur. More quantitatively, us-

ing Eq.(7) one gets that

$$\begin{aligned}
N_{24,42}(t) &= \frac{1}{2} - 4g^2 J'^2 \frac{\sin^2[\omega_{13}t/2]}{\hbar^2 \omega_{13}^2} \\
&\quad \pm \frac{\omega_1 \cos(\omega_3 t) - \omega_3 \cos(\omega_1 t)}{2\omega_{13}} \\
N_{33}(t) &= 8g^2 J'^2 \frac{\sin^2[\omega_{13}t/2]}{\hbar^2 \omega_{13}^2} \quad (9)
\end{aligned}$$

Here  $\omega_{13} = \omega_1 - \omega_3$ . In the limit  $\Delta_b \gg J'$ ,  $\omega_3$  dominates over  $\omega_1$ , the  $|3, 3\rangle$  states are only virtually populated and the above expressions reduce to

$$N_{24,42}(t) = \frac{1}{2} (1 \pm \cos(\omega_1 t)) \quad N_{33}(t) \approx 0 \quad (10)$$

### Derivation of the Effective Hamiltonian parameters: Multi-plaquette case

The microscopic parameters of the many-plaquette Hamiltonian are more complicated than the ones in Eq.(4) since in addition to the virtual couplings between  $|4_R, 2_{R+1}\rangle \leftrightarrow |2_R, 4_{R+1}\rangle$  through tunneling to  $|3_R, 3_{R+1}\rangle$  (which are inversely proportional to  $\Delta_b$ ), when many plaquettes are coupled, there are additional processes that one must consider: We have to include the couplings between  $|4_R, 4_{R+1}\rangle \leftrightarrow |4_R, 4_{R+1}\rangle$  mediated by  $|5_R, 3_{R+1}\rangle$  states and between  $|2_R, 2_{R+1}\rangle \leftrightarrow |2_R, 2_{R+1}\rangle$  mediated by  $|3_R, 1_{R+1}\rangle$  (which are inversely proportional to  $g_4^2/\Delta_{44}$  and  $g_2^2/\Delta_{44}$  where  $\Delta_{44} = E_5 + E_3 - 2E_4$ ,  $\Delta_{22} = E_3 + E_1 - 2E_2$  and  $g_{4,2}$  are corresponding coupling matrix elements). Since the energy gaps  $\Delta_{44}$  and  $\Delta_{22}$  are about one order of magnitude larger than  $\Delta_b$ , to be consistent, one has in addition to sum over all possible higher energy virtually populated states (leading to additional corrections we denote by  $\delta$ ). All these processes give rise to an effective coupling constant along the axial direction given by:  $g_z^2 = g^2 - \frac{g_2^2 \Delta_b}{2\Delta_{22}} - \frac{g_4^2 \Delta_b}{2\Delta_{44}} + \delta$

### Initial preparation of the plaquettes with $N_2 = 2N_4$

The preparation starts by loading a unit filled band insulator of fermionic atoms in a rectangular lattice with lattice period  $3/2\lambda$  and  $\lambda$  along the  $x$  and  $y$  direction respectively. After this, the  $\lambda$  lattice is ramped up along  $x$  simultaneously with a weaker  $3\lambda$  lattice. While the former creates an additional well in between two initially populated wells, the latter provides an energy offset to guarantee that the new wells remain unpopulated. Next, one has to slowly turn off the  $3/2\lambda$  lattice while turning on a  $2\lambda$  lattice. At the end of this procedure one has generated a distribution of double wells along  $x$  with the appropriated bias such that the ground state population has 242

pattern. After increasing the lattice depth of the  $2\lambda$  lattice until all wells are made independent one can suddenly turn off the  $3\lambda$  lattice which provided the bias without causing any excitation. The overall scheme creates an array of independent plaquettes loaded in the ground state with alternating filling factors of 2, 4, 2 along the  $x$  direction.

### Noise Correlations

Here we provide explicit expressions for the noise correlations shown in Fig.6. These expressions can be derived using the fact that the states to probe are linear superpositions of states populated with only 4 and 2 fermions in each plaquette, and therefore that they can be mapped to an effective spin 1/2 system. Using this simplification, the noise correlations can be written as

$$G^{\uparrow\downarrow}(\mathbf{Q}, \mathbf{Q}') \propto A(\mathbf{Q}, \mathbf{Q}') + \mathbf{S}^{+-}(\mathbf{Q} + \mathbf{Q}') \mathcal{D}(\mathbf{Q}, \mathbf{Q}') \quad (11)$$

$$\begin{aligned}
G^{\uparrow\uparrow}(\mathbf{Q}, \mathbf{Q}') &\propto A(\mathbf{Q}, \mathbf{Q}') - F^+(\mathbf{Q}, \mathbf{Q}') \delta(\mathbf{Q} - \mathbf{Q}' - m\mathbf{K}) \\
&\quad - S^{zz}(\mathbf{Q} - \mathbf{Q}') F^-(\mathbf{Q}, \mathbf{Q}') \quad (12)
\end{aligned}$$

The term  $A$  corresponds to trivial diagonal density-density correlations within a plaquette and ideally one could subtract this term from the measured noise pattern.  $\mathbf{S}^{+-}(\mathbf{Q} + \mathbf{Q}') = \sum_{\mathbf{R} \neq \mathbf{R}'} e^{i(\mathbf{Q} + \mathbf{Q}') \cdot (\mathbf{R} - \mathbf{R}')} \langle \sigma_{\mathbf{R}}^+ \sigma_{\mathbf{R}'}^- \rangle$  is the analog of the quasi-momentum distribution when one maps the spins to hardcore bosons and consequently probes the long range order. If the system is a  $d$ -wave superfluid  $\mathbf{S}^{+-}(\mathbf{Q} + \mathbf{Q}')$  will exhibit sharp interference peaks at  $\mathbf{Q} + \mathbf{Q}' = \mathbf{K}n$ ,  $\mathbf{K}$  being the reciprocal lattice vector of the plaquette array, which is half of the reciprocal lattice vector of the underlying lattice. On the contrary  $\mathbf{S}^{+-}(\mathbf{Q} + \mathbf{Q}')$  will have a flat profile in the case of a  $d$ -cdw state. The term  $\mathcal{D}(\mathbf{Q}, \mathbf{Q}') = \left| \sum_{r, r'} e^{i(\mathbf{Q} \cdot \mathbf{l}_r + \mathbf{Q}' \cdot \mathbf{l}_{r'})} \langle 2 | c_r^\dagger c_{r'}^\dagger | 4 \rangle \right|^2$  probes non-diagonal local plaquette correlations ( $r, r'$  label sites within the same plaquette) and gives information about the  $d$ -wave nature of the superfluid.  $\mathcal{D}(\mathbf{Q}, \mathbf{Q}')$  modulates the  $\mathbf{S}^{+-}(\mathbf{Q} + \mathbf{Q}')$  peak structure inducing the characteristic  $d$ -wave nodal lines along  $Q_x = \pm Q_y$  and  $Q'_x = \pm Q'_y$ , where the signal vanishes due to the  $d$ -wave symmetry of the Cooper pairs (see Fig.6).

Information about the density order is given by  $G^{\uparrow\uparrow}$ .  $S^{zz}(\mathbf{Q} - \mathbf{Q}') = \sum_{\mathbf{R} \neq \mathbf{R}'} e^{i(\mathbf{Q} - \mathbf{Q}') \cdot (\mathbf{R} - \mathbf{R}')} \langle \sigma_{\mathbf{R}}^z \sigma_{\mathbf{R}'}^z \rangle$  shows sharp peaks at  $\mathbf{Q} = \mathbf{Q}' + (2n + 1)\mathbf{K}/2$  in the presence of a  $d$ -cdw phase and a flat profile in the superfluid phase. In contrast to the unequal spin correlations the terms  $F^\pm(\mathbf{Q}, \mathbf{Q}')$  do not have the inherent  $d$ -wave symmetry. They are just geometric factors that depend on the kinetic energy within the isolated plaquettes:  $F^\pm(\mathbf{Q}, \mathbf{Q}') = |\alpha_4(\mathbf{Q}, \mathbf{Q}') \pm \alpha_2(\mathbf{Q}, \mathbf{Q}')|^2/4$  with  $\alpha_n(\mathbf{Q}, \mathbf{Q}') = \sum_{r, r'} e^{i(\mathbf{Q} \cdot \mathbf{l}_r - \mathbf{Q}' \cdot \mathbf{l}_{r'})} \langle n | c_r^{\sigma\dagger} c_{r'}^\sigma | n \rangle$ , and  $n = 2, 4$ . The delta function  $\delta(\mathbf{Q} - \mathbf{Q}' - m\mathbf{K})$  reflects the characteristic anti-bunching of fermions.